EFFECTS OF PCO_2 AND IRON ON THE ELEMENTAL COMPOSITION AND CELL GEOMETRY OF THE MARINE DIATOM *PSEUDO-NITZSCHIA PSEUDODELICATISSIMA* (BACILLARIOPHYCEAE)[1]

Koji Sugie,[2] and Takeshi Yoshimura

[2:] Central Research Institute of Electric Power Industry, 1646 Abiko, Abiko, Chiba 270-1194, Japan

[2]: Author for correspondence:
Koji Sugie
Present address: Faculty of Environmental Earth Sciences, Hokkaido University, West-5, North-10, Kita-ku, Sapporo, Hokkaido, 060-0810, Japan
E-mail: kojisugie@gmail.com
Tel&Fax: +81-11-706-2370

Running head: Effects of pH and Fe on diatom

ABSTRACT

Partial pressure of CO_2 (pCO_2) and iron availability in seawater show corresponding changes due to biological and anthropogenic activities. The simultaneous change in these factors precludes an understanding of their independent effects on the ecophysiology of phytoplankton. In addition, there is a lack of data regarding the interactive effects of these factors on phytoplankton cellular stoichiometry, which is a key driving factor for the biogeochemical cycling of oceanic nutrients. Here, we investigated the effects of pCO_2 and iron availability on the elemental composition (C, N, P and Si) of the diatom *Pseudo-nitzschia pseudodelicatissima* (Hasle) Hasle by dilute batch cultures under 4 pCO_2 (~200, ~380, ~600, and ~800 µatm) and 5 dissolved inorganic iron (Fe′; ~5, ~10, ~20, ~50, and ~100 pmol L^{-1}) conditions. Our experimental procedure successfully overcame the problems associated with simultaneous changes in pCO_2 and Fe′ by independently manipulating carbonate chemistry and iron speciation, which allowed us to evaluate the individual effects of pCO_2 and iron availability. We found that the C:N ratio decreased significantly only with an increase in Fe′, whereas the C:P ratio increased significantly only with an increase in pCO_2. Both Si:C and Si:N ratios decreased with increasing pCO_2 and Fe′. Our results indicate that changes in pCO_2 and iron availability could influence the biogeochemical cycling of nutrients in future oceans with high CO_2 levels, and, similarly, during the time course of phytoplankton blooms. Morever, pCO_2 and iron availability may also have affected oceanic nutrient biogeochemistry in the past, as these conditions have changed markedly over the Earth's history.

Key index words: carbon dioxide, cell size, diatom, elemental composition, iron, nutrients, ocean acidification

Abbreviations: BSi, biogenic silica; CCMs, carbon concentration mechanisms; CV, cell volume; DIC, dissolved inorganic carbon; Fe′, dissolved inorganic iron; k_μ, half-saturation constant for growth; pCO_2, partial pressure of CO_2; PN, particulate nitrogen; POC, particulate organic carbon; PP, particulate phosphate; SA, surface area;

TA, total alkalinity; VA_{ratio}, valve aspect ratio; xCO_2, concentration of CO_2; α, initial slope of Monod kinetics; μ_{max}, maximum specific growth rate

INTRODUCTION

The dissolution of CO_2 that is primarily emitted from anthropogenic activities causes the partial pressure of CO_2 (pCO_2) to increase and the pH to decrease in surface oceans. Ocean pH has decreased by ~0.1 unit since preindustrial times and will continue to decrease as long as fossil fuels are burned without significant efforts to reduce the atmospheric CO_2 (Doney et al. 2009). The rate of pH decline during the Anthropocene (beginning in the late 18th century; Crutzen 2002) is probably considerably more rapid than that which occurred over the past several tens of millions of years (Doney et al. 2009). Concomitant with ocean acidification, the ferrous to ferric iron composition (Millero et al. 2009) and the conditional stability constant of iron-ligand complexes (Shi et al. 2010) could increase in the future as atmospheric CO_2 rises. In addition to increasing atmospheric CO_2, other human perturbations, such as land use and SO_x and NO_x emissions, will further alter iron distribution and bioavailability in the open ocean (Mahowald et al. 2009). Therefore, ocean acidity and iron availability will show corresponding changes in future high-CO_2 oceans. Based on this finding, experiments that use natural seawater will not be able to distinguish the impact of carbonate chemistry or iron bioavailability on phytoplankton ecophysiology.

A critical challenge is to understand how the rapid decline in pH during the Anthropocene era affected phytoplankton ecophysiology. However, the atmospheric CO_2 concentrations during the Quaternary period (~1.8 million years ago to the present; Gradstein et al. 2004) have been close to their lowest level (180–390 ppm; Doney et al. 2009) during the past 60 million years (<~4000 ppm; Pearson and Palmer 2000). Most marine phytoplankton groups had already evolved prior to the decline in the levels of CO_2 in the atmosphere and oceans (Falkowski et al. 2004). Therefore, diatoms, which are the predominant primary producers in the present oceans (Falkowski et al. 2004), and many other algae, have adapted to the low CO_2 conditions by developing CO_2 concentration mechanisms (CCMs). These mechanisms elevate the substrate

concentration around the enzyme RubisCO, which is involved in CO_2 fixation (Hopkinson et al. 2011; Reinfelder 2011; and references therein). The upregulation of CCMs may incur substantial energy and nutrient costs. Therefore, an increase in pCO_2 may result in decreased CCMs cost, resulting in the enhanced growth of diatoms and other algae (Hutchins et al. 2009; Hopkinson et al. 2010). This physiological plasticity alters the composition of biochemical constituents such as the components of CCMs and can modify the cellular elemental composition associated with macromolecular stoichiometry (Geider and La Roche 2002).

Previous studies have reported that an increase in seawater pCO_2 alters the physiology and cellular elemental composition or nutrient consumption ratio of diatoms (Burkhardt et al. 1999, Sun et al. 2011), dinoflagellates, raphidophytes (Fu et al. 2008), cyanobacteria (Fu et al. 2007), and plankton communities in a mesocosm enclosure (Riebesell et al. 2007). For example, high pCO_2 conditions accelerated photosynthesis of many phytoplankton species (e.g. Rost et al. 2003, Sun et al. 2011) and the N_2-fixation rates of N_2-fixing cyanobacteria (e.g. Hutchins et al. 2007, Levitan et al. 2007). Other studies using unialgal cultures showed that the C:P ratio increased, and the Si:C ratio decreased, in diatoms, dinoflagellates, raphidophytes, and cyanobacteria with increasing pCO_2 in seawater (Fu et al. 2007, Fu et al. 2008, Sun et al. 2011). However, the C:N ratio was relatively unaffected by changes in seawater pCO_2. It should be noted that most of these studies were conducted under conditions with abundant macronutrients and trace elements, such as iron. However, although it is widely recognized that the primary productivity is limited by iron in large areas of the ocean (de Baar 1994, Saito et al. 2008), the interactive effects of pCO_2 and iron on the elemental composition of phytoplankton have not been examined.

Iron is an essential trace element for phytoplankton growth because of its role in key metabolic processes such as photosynthesis, respiration, and nitrate and nitrite assimilation (Raven et al. 1999). The iron found in oceanic regions is mainly derived from continental sources; however, iron has an extremely low solubility in oxic surface seawater (<~0.1 nmol L^{-1}; Kuma et al. 1996). Therefore, the phytoplankton, particularly diatoms, in the oceanic regions located far from iron sources are iron-limited (de Baar

1994). In addition, the iron concentration varies spatiotemporally by one to two orders of magnitude due to water mass exchange and biological uptake in the western subarctic Pacific (Sugie et al. 2010a, Nishioka et al. 2011). Therefore, phytoplankton need to adapt and survive in a fluctuating iron environment (Sugie and Kuma 2008, Sugie et al. 2011). Changing iron availability results in changes in the elemental composition of the diatoms; specifically, the cellular Si:N ratio increases as iron bioavailability decreases (e.g. Takeda 1998). The following mechanisms have been suggested for this increase in Si:N ratio: (i) an increase in silicification or resting spore formation (e.g. Sugie et al. 2010b); (ii) an increase in surface area (SA) to cell volume (CV) ratio (Marchetti and Harrison 2007); (iii) a reduction in cellular N content (e.g. Takeda 1998); and (iv) a response to the high Si:N ratio or high Si concentration of the extracellular environment (Kudo 2003, Finkel et al. 2010a). A recent study reported that the relationship between elemental composition and the bioavailable iron concentration is not always linear (Bucciarelli et al. 2010). Therefore, culture experiments should be conducted over a wide range of iron concentrations to improve our understanding of the stoichiometry of phytoplankton as it relates to changes in iron availability. In addition, simultaneous measurements of the C, N, P, and Si composition of diatoms have rarely been conducted despite their importance.

In the present study, we describe a new method for evaluating the individual effects of pCO_2 and iron availability on marine phytoplankton ecophysiology. We investigated the interactive effects of pCO_2 and iron on the elemental compositions (C, N, P and Si) and cell geometry of the diatom *Pseudo-nitzschia pseudodelicatissima* (Hasle) Hasle. *Pseudo-nitzschia* species are ubiquitous, even in iron-depleted oceanic environments (Hasle 2002, de Baar et al. 2005). Therefore, species of the genus *Pseudo-nitzschia* are among the most suitable diatoms for examining the interactive effects of pCO_2 and iron in order to understand the biogeochemical cycling of nutrients in high-CO_2 oceans.

MATERIALS AND METHODS

149 *Diatom strain and culture conditions*. Seawater for the culture medium was
150 collected from Onjuku, Chiba, Japan (35°18′N, 140°38′E). Salinity of the seawater was
151 34.2. Initially, the seawater was filtered through a 0.22 µm cartridge filter (Advantech
152 Co. Ltd., Tokyo, Japan). Macronutrients were then added to the filtered seawater and the
153 seawater was aged for ~1 month in an acid-washed 50 L polypropylene carboy, to
154 precipitate dissolved iron, excess to its solubility, as conducted previously (Sugie et al.
155 2010b). Stock solutions of macronutrient were passed through a Chelex 100 resin
156 (Bio-Rad, CA, USA) to remove trace metals, as described by Price et al. (1988/89). The
157 filtered seawater was then passed through a 0.1 µm filter (Merck Millipore, MA, USA)
158 to sterilize it and to eliminate particulate iron prior to use. The background iron
159 concentration of the filtered seawater was 0.47 nmol L^{-1}, as measured by flow-injection
160 with chemiluminescence detection (Obata et al. 1993).
161 Seawater for the isolation of *P. pseudodelicatissima* was collected from Harima
162 Nada, Seto Island Sea, Japan (34°77′N, 134°70′E) in 2009. The experiment was
163 conducted within 1.5 years after isolation. A single cell was isolated using a capillary
164 pipette and rinsed several times with 0.1 µm filtered seawater. Although, the strain was
165 not completely axenic, bacterial contamination was minimized by the use of sterile
166 techniques and serial transfer during exponential growth. To identify the species, the
167 diatom cell was cleaned according to the method described by Nagumo (1995), and the
168 cleaned frustule was observed using a scanning electron microscope. Species
169 identification was performed according to Hasle and Syvertsen (1997). The strain was
170 maintained in modified Aquil medium (Price et al. 1988/89) at 20°C under Neolumisuper
171 fluorescent light at 100 µmol photons m^{-2} s^{-1} (FLR40S•W/M, Mitsubishi Electric Osram
172 Ltd., Yokohama, Japan), measured using QSL radiometer (Biospherical Instrument Inc.,
173 CA, USA), and 12h light:12 h dark. The light intensity was measured at the center of the
174 culture bottle. The modified Aquil medium was composed of 0.1 µm filtered seawater,
175 ~100 µmol L^{-1} NO_3^-, ~6 µmol L^{-1} PO_4^-, ~150 µmol L^{-1} $Si(OH)_4$, and Aquil metals
176 chelated with 100 µmol L^{-1} of EDTA. Because 100 µmol L^{-1} of EDTA can out-compete
177 any natural ligand that may be present in the medium (Gerringa et al., 2000), the iron
178 (including background iron) in the culture medium should be in equilibrium with EDTA.

179 The iron, other trace metals, and EDTA stock solutions were mixed in 1 L polycarbonate
180 culture bottles before the addition of 1 L of modified Aquil medium. All equipment used
181 in the culture experiment was acid-washed (soaked for at least 24 h in either 1 or 4 mol
182 L^{-1} HCl solution; 1 mol L^{-1} HCl was used for polycarbonate bottles) followed by rinsing
183 thoroughly with Milli-Q water (>18.0 MΩ cm^{-1}, Merck KGaA, Darmstadt, Germany).
184 Preparation and sampling for all experiments were conducted in a class 1000 clean room
185 and at a class 100 clean bench, respectively, to avoid inadvertent trace metal
186 contamination.
187 *Experimental design*. Carbonate chemistry during the culture experiment was
188 manipulated by injecting controlled dry air with a specific CO_2 concentration (xCO_2)
189 (Nissan Tanaka Corp., Saitama, Japan) directly into the culture bottles at a flow rate of
190 ~10 mL min^{-1}. The injected air was passed through a 0.2 μm in-line filter to avoid
191 contamination from the gas cylinder or lines and humidified by passing the gas through
192 Milli-Q water. The xCO_2 of the injected air was set at 171, 386, 614, and 795 ppm,
193 corresponding to the glacial minimum, present, and two possible future CO_2 conditions,
194 respectively (Table 1). For each CO_2 condition, five concentrations of dissolved
195 inorganic iron species (Fe′), representing ~50–100% of the maximum growth rate of *P.*
196 *pseudodelicatissima* (μ_{max} = ~1.9 d^{-1}), were used: 3.5, 7.0, 18, 30 and 70 pmol L^{-1}. The
197 concentrations correspond to pFe′ (= $-\log_{10}$[Fe′]) of 11.5, 11.1, 10.8, 10.5, and 10.2,
198 respectively (Table 1). The Fe′ concentration was calculated according to Sunda and
199 Huntsman (2003). When calculating Fe′ concentrations, background iron was included
200 with the added iron (see above). Because the iron-EDTA buffer system is pH sensitive
201 (Sunda and Huntsman 2003), the defined Fe′ concentrations were obtained by
202 recalculation using pH values that were calculated from the dissolved inorganic carbon
203 (DIC) and total alkalinity (TA) data. The DIC and TA were measured at the start and end
204 of the experiment (Table 1). To achieve steady state and equilibrium of the carbonate
205 chemistry and iron-EDTA system, xCO_2 controlled air was bubbled into the modified
206 Aquil medium at a flow rate of ~30 mL min^{-1} for 3–4 days before the addition of the
207 diatom cells. Experiments were conducted in duplicate bottles maintained under the
208 same temperature and light conditions as the stock cultures.

Prior to initiating the culture experiment, *P. pseudodelicatissima* cells were acclimated to the four CO_2 conditions stated above, under high (70 pmol L^{-1}) or low (4.0 pmol L^{-1}) Fe′ conditions. The acclimation period was 9 days, corresponding to ~20 and ~10 cell divisions for the high and low Fe′ conditions, respectively. In the culture experiment, cells acclimated under high Fe′ conditions were used for the two higher Fe′ treatments, while cells acclimated under low Fe′ conditions were used for the three lower Fe′ treatments. Approximately 50–100 cells mL^{-1} were added to each medium at the beginning of the experiment. Cells were cultured by dilute batch culture and were harvested at less than 5% of the carrying capacity of the modified Aquil medium. The diatoms were cultured in the experimental media for 4–6 days while they were still in exponential growth, a period that corresponded to between the 7th and 10th cell division under experimental conditions.

Growth rate, cell size and geometry. Growth was monitored daily using a Multisizer 4 Coulter Counter (Beckman Coulter Inc., CA, USA) to calculate the specific growth rate. Because *P. pseudodelicatissima* forms chains, we measured the biovolume of each sample at least three times. Specific growth rates were calculated from the linear regression between the natural log of the biovolume and time (day). The maximum specific growth rate (μ_{max}) and half saturation constant for growth (k_μ) were obtained by nonlinear fitting of the growth rate and Fe′ data to the Monod equation (e.g., Sarthou et al. 2005). The initial slope of the growth rate to Fe′ curve (α) was calculated as μ_{max} divided by k_μ (e.g. Healey 1980). In addition, we calculated the net elemental (E) uptake rate (ρ) per unit SA to account for the effect of the difference in cell size on nutrient uptake ability as follows; $\rho E_{SA} = Q_E \times \mu \div SA$, where Q_E represents cell quota of C, N, P, or Si. The maximum ρE_{SA} ($\rho E_{SA\text{-}max}$) and the half saturation constant for net uptake rate ($k\rho$) values against Fe′ concentration were obtained using a method similar to that for specific growth rate. The $\rho E_{SA\text{-}max}$ and $k\rho$ represent the maximum possible nutrient uptake ability per unit SA and the sensitivity of nutrient uptake transporter sites against the Fe′ concentrations (i.e., uptake affinity), respectively. At the end of the culture experiment, a small amount of each of the samples was fixed with neutralized formalin (~1% final volume) to measure the cell number and geometry. The cell number was

239 counted four times per sample using a Fuchs-Rosenthal hemacytometer (Erma Inc.,
240 Tokyo, Japan) at ×200 magnification using a differential interference contrast equipped
241 microscope (Olympus Corp., Tokyo, Japan). The apical length and transapical or
242 pervalver lengths of up to 20 cells from one of the duplicate bottles were measured to
243 calculate the CV and SA by using digital images of the cells and an objective micrometer
244 at ×400 fold magnification (Sun and Liu 2003). Geometric calculations of the CV and
245 SA were performed according to the equation suggested by Marchetti and Harrison
246 (2007). The valve aspect ratio was calculated by dividing the apical length by the
247 transapical or pervalver length of the cell.
248 *Chemical analyses*. The DIC and TA were measured at the start and end of the
249 experiment using a potentiometric Gran plot method with dilute HCl (0.1 mol L^{-1}; Wako
250 Co. Ltd., Osaka, Japan) and a total alkalinity analyzer (Kimoto electric Co. Ltd., Osaka,
251 Japan), as described by Edmond (1970). However, as the EDTA began absorbing protons
252 below pH ~4, the titration data below pH 4 were eliminated from the Grand plot. The
253 stability of the titration analysis was checked using DIC reference material (KANSO Co.
254 Ltd., Osaka, Japan), which the DIC value was traceable to the certified reference
255 materials supplied by Andrew Dickson, University of California, San Diego, USA. The
256 analytical errors were <0.1% for DIC (~1.1 μmol kg^{-1}) and TA (~1.4 μmol kg^{-1}). At the
257 end of the culture period, macronutrients were measured using a QuAAtro-2 continuous
258 flow analyzer (Bran+Luebbe, SPX Corp., NC, USA). At the end of the experiment, cells
259 were harvested on a precombusted GF/F filter for particulate organic carbon (POC),
260 particulate nitrogen (PN), and particulate phosphorus (PP) analysis. Cells were harvested
261 on a polycarbonate membrane filter (pore size, 0.8 μm) for biogenic silica (BSi) analysis.
262 Filter samples for POC and PN were freeze-dried, and the concentrations were measured
263 using a CHN analyzer (Perkin Elmer Inc., MA, USA). PP was measured using a
264 spectrophotometer (Hitachi High-Teck Corp. Tokyo, Japan) after high temperature
265 combustion and acid hydrolysis of the filters as described by Solórzano and Sharp (1980).
266 For BSi analysis, the filter was digested by heating to 85°C for 2 h in 0.5% Na_2CO_3
267 solution (Paasche, 1980). After neutralizing with 0.5 mol L^{-1} HCl, the silicic acid
268 concentration was measured using a QuAAtro-2 continuous flow analyzer. All data for

POC, PN, PP and BSi concentrations were corrected by subtracting values obtained from appropriate filter blanks. Cellular elemental concentrations (C, N and P) were calculated by dividing POC, PN, or PP concentrations by cell density and CV. The SA normalized Si as an indicator of frustule thickness was calculated by dividing BSi concentration by cell density and SA.

Statistics. Data trends obtained under different pCO_2 and iron conditions were evaluated using *F*-tests, and regression coefficients were evaluated using *t*-tests. The regression formula was chosen to achieve the highest accuracy (i.e., *F* value and correlation coefficient). Data for fitting the Monod equation were calculated using Origin software (version 8.0, OriginLab Corp., MA, USA) with a non-linear method. Multi-regression analyses were conducted using PASW statistics software (version 17.0, SPSS Inc., IL, USA). Significant results are reported at the 95% confidence level.

RESULTS

Medium conditions. At the beginning of the experiment, seawater pCO_2 was close to steady state with the xCO_2 of the bubbled air in the three higher CO_2 bottles (412 ± 8, 609 ± 11 and 769 ± 11 µatm), whereas a slightly higher value than the expected steady state value was observed in the lowest xCO_2 treatment (251 ± 17 µatm) (Table 1). The corresponding pH values (represented as mean ± range of duplicate bottles) for the 171, 386, 614, and 795 ppm xCO_2 treatments were 8.22 ± 0.02, 8.05 ± 0.01, 7.90 ± 0.01, and 7.81 ± 0.01, respectively. During the course of the experiment, the DIC decreased due to phytoplankton growth that exceeded DIC addition by bubbling. The decrease in DIC was greater in treatments with high Fe′ conditions and 171 ppm xCO_2 treatments than that in low Fe′ conditions and higher xCO_2 treatments because photosynthesis and the bubbling of low xCO_2 air simultaneously depressed DIC. At the end of the culture period, the pCO_2 had decreased by ~30–300 µatm, while the pH had increased by 0.03–0.20 units, depending on the extent of phytoplankton growth (Table 1). Further, during the experiment, the Fe′ changed due to the increase in pH. The change in Fe′ ranged from ~15% under the low Fe′ conditions to 100–140% under the high Fe′ conditions (Table 1). We used the means of the initial and final pCO_2 and Fe′ values for

299 the subsequent data analysis. The macronutrient levels remained sufficient [~100 μmol
300 L^{-1} NO_3^-+NO_2^-; ~5.5 μmol L^{-1} PO_4^-; and ~145 μmol L^{-1} $Si(OH)_4$] for phytoplankton
301 growth at the end of the experiment.
302 *Growth rate, cell size, and geometry*. The specific growth rate increased with Fe′
303 concentration from ~1.0 to ~2.0 d^{-1} (Fig. 1A). Multi-regression analysis indicated that
304 the specific growth rate was strongly correlated with Fe′ but not with pCO_2, within the
305 investigated ranges (Table 2). The μ_{max} values for the 171, 386, 614 and 795 ppm xCO_2
306 treatments calculated using the Monod equation were 1.81 ± 0.03, 1.89 ± 0.03, 2.06 ±
307 0.04, and 1.98 ± 0.05, respectively. The k_μ values for the four xCO_2 treatments were 1.48
308 ± 0.18, 3.64 ± 0.35, 4.97 ± 0.39 and 4.23 ± 0.55 pmol Fe′ L^{-1}, respectively. The initial
309 slope of the Monod regression (α) was highest for the 171 ppm xCO_2 treatment and
310 decreased with increasing pCO_2 (Fig. 2). The CV showed a gradual, although significant,
311 increase with increasing Fe′ and decreasing pCO_2 (Fig. 1B, Table 2). CV was positively
312 correlated with specific growth rate (Fig. 1C) and varied with the length of the
313 transapical or pervalver axis but not with the length of the apical axis (Fig. 1D, E).
314 Therefore, SA/CV was tightly regulated by the valve aspect ratio (VA_{ratio}; Fig. 1F). The
315 lengths of the apical axis and transapical or pervalver axis were not significantly
316 influenced by variations in pCO_2. VA_{ratio} and SA/CV significantly increased with
317 increasing pCO_2 and decreased with increasing Fe′ concentrations (Table 2). Further,
318 although *P. pseudodelicatissima* cells were acclimated to only two Fe′ regimes, they
319 appeared to be fully acclimated to the experimental conditions because the results
320 indicated gradual changes in the growth rate, cell size, and geometry with respect to the
321 Fe′ variation.
322 *Cellular C, N, P, and Si*. The highest intracellular (In_{cell}) C and N concentrations
323 and the SA normalized BSi concentration (Si/SA), were measured at 10.6–10.2 pFe′
324 (25–63 pmol L^{-1}), when the growth rates were 80–95% of μ_{max} (Fig. 3). The empirical
325 equation for each element (C, N, P, and Si) was obtained from the data in Figure 3 as
326 follows:
327 In_{cell} [C] (mol L^{-1}) = −863 + (166 × pFe′) − (7.86 × pFe′^{2}) ($F_{2,37}$ = 21.9, p < 0.001) (1)
328 In_{cell} [N] (mol L^{-1}) = −134 + (26.1 × pFe′) − (1.24 × pFe′^{2}) ($F_{2,37}$ = 35.7, p < 0.001) (2)

In_{cell} [P] (mmol L^{-1}) = (-7.35×10^{-3}) + ($1464 \times pFe'$) − ($70.9 \times pFe'^2$) + ($0.101 \times pFe' \times pCO_2$) − ($1.21 \times pCO_2$) ($F_{4,35} = 18.2$, $p < 0.001$) (3)

[Si]/SA (mmol m^{-2}) = $-112 + (21.4 \times pFe') - (1.03 \times 10^{-3} \times pCO_2) - (1.00 \times pFe'^2)$ ($F_{3,36} = 28.6$, $p < 0.001$) (4)

The In_{cell} C, N, and P concentrations and Si/SA graphs had quadric surfaces with respect to the pFe′. However, changes in pCO_2 linearly affected only the In_{cell} P and Si/SA concentrations while changes in *p*CO2 were not significantly associated with In_{cell} C and N concentrations. Si/SA decreased significantly with increasing pCO_2 ($t = -5.8$, $p < 0.001$, df = 39). In contrast, In_{cell} P concentration increased significantly with decreasing pCO_2 ($t = -2.9$, $p = 0.006$, df = 39).

In general, the highest ρE_{SA} was detected for the 171 and 386 ppm xCO_2 treatments under high Fe′ conditions, whereas the lowest ρE_{SA} was measured for the high-CO_2 and low-Fe′ conditions (Fig. 4). All regression coefficients, with the exception of ρN_{SA} for pCO_2 were significant (Table 2); the ρC_{SA}, ρP_{SA}, and ρSi_{SA} increased with increasing Fe′ concentration and decreasing with increasing pCO_2 (Fig. 4A, C, D). In contrast, ρN_{SA} was affected only by iron availability and increased with increasing Fe′ (Fig. 4B, Table 2). The maximum ρE_{SA} ($\rho E_{SA\text{-}max}$) and half saturation constant for the ρE_{SA} (k_ρ) as a function of Fe′ were determined by fitting the data with the Monod model (Table 3). The highest $\rho E_{SA\text{-}max}$ values of ρC_{SA}, ρP_{SA}, and ρSi_{SA} were obtained for the 171 ppm xCO_2 treatment, whereas those for the 614 and 795 ppm xCO_2 treatments were similar. The $\rho E_{SA\text{-}max}$ of ρN_{SA} was not affected by pCO_2 variation (Table 3). The highest α values of ρC_{SA}, ρN_{SA}, and ρP_{SA} were obtained for the 171 ppm xCO_2 treatment, whereas the other three xCO_2 treatments had similar α values (Table 3).

Elemental composition. The cellular C:N ratio significantly increased from ~5.9 to ~6.5 as Fe′ concentration decreased, while the coefficient for pCO_2 was not statistically significant (Fig. 5A, Table 2). In contrast, the cellular C:P ratio significantly increased with increasing pCO_2, but not with Fe′ concentration (Fig. 5B, Table 2). The average cellular C:P ratios (mean ± 1SD of ten replicates) for the 171, 386, 614, and 795 ppm xCO_2 treatments were 98 ± 9.0, 119 ± 22, 136 ± 31, and 139 ± 15, respectively (Fig. 5B). The cellular N:P ratio was positively correlated with pCO_2 and Fe′ and ranged from

~15 in the low pCO_2 and Fe′ conditions to ~26 in the high pCO_2 and Fe′ conditions (Fig. 5C, Table 2). The cellular Si:N and Si:C ratios decreased significantly as pCO_2 and Fe′ concentration increased (Fig. 5D, E, Table 2). The cellular Si:P ratio was positively correlated with pCO_2, but negatively correlated with Fe′ (Fig. 5F, Table 2).

DISCUSSION

We demonstrated that the elemental composition and cell geometry of the marine diatom *P. pseudodelicatissima* are influenced by variations in pCO_2, Fe′ or a combination of both factors. In addition, we found that the elemental composition of cells changed linearly with pCO_2 and $\log_{10}$[Fe′]. It is important to distinguish between the effects of these factors when evaluating the results obtained using natural phytoplankton communities particularly under iron-limited conditions. This is because carbonate chemistry and iron bioavailability can change simultaneously in natural seawater (Millero et al. 2009; Shi et al. 2010). These simultaneous changes preclude understanding of their independent effects on phytoplankton ecophysiology. By manipulating the carbonate chemistry and iron speciation independently, we overcome this problem and evaluated the individual effects of pCO_2 and iron availability.

Growth rate, cell size and geometry. We found that the specific growth rate and the theoretical maximum specific growth rate (μ_{max}) were not affected by pCO_2. These results are similar to those of a recent study of eight phytoplankton species belonging to four phyla (Berge et al. 2010). Trimborn et al. (2008) reported that *Pseudo-nitzschia multiseries* has a highly efficient CCMs and the activity of the CCMs may increase in response to a decrease in DIC availability. Because the use of CCMs may consume a substantial part of the energy for growth (Hopkinson et al. 2010, 2011), the increase in CO_2 availability may benefit phytoplankton (Hutchins et al. 2009). Shi et al. (2010) reported that the cellular iron requirements (Fe:C ratio) of model diatom species (*Thalassiosira pseudonana*, *Thalassiosira weissflogii*, and *Phaeodactylum tricornutum*) seem to increase under low CO_2 (160 ppm) conditions possibly because of the need to upregulate CCMs. CCMs are energy-using processes that require ATP. If this ATP is supplied by PSI cyclic photophosphorylation (cf. Raven 1999, Allen 2003, Beardall et al.

2005), the high Fe content of the PSI and the associated cyclic electron transport pathway may increase the iron requirement of diatoms when CCMs are upregulated under conditions of low CO_2 availability. Further, our results show that iron uptake affinity (α) increased with decreasing pCO_2 (Fig. 2). This supports the idea that the energy demand for the development of the CCMs increases when pCO_2 decreases (Beardall et al. 2005, Young and Beardall 2005, Hopkinson et al. 2011). In addition, we observed a relatively high uptake affinity and maximum uptake rate for C and nutrients by *P. pseudodelicatissima* cells grown under the lowest pCO_2 condition. The ability of the cells to develop high affinity iron transport and elevated C and nutrient uptake under conditions of low CO_2 availability may partly overcome the less favorable growth conditions.

Interestingly, the cell volume (CV) of *P. pseudodelicatissima* increased significantly as pCO_2 decreased. Theoretically, CV increases under substrate replete conditions (e.g. Thingstad et al. 2005, Finkel et al. 2010b). In the present study, CV decreased as iron availability decreased as observed elsewhere (Marchetti and Harrison 2007, Sugie and Kuma 2008). Furthermore, CV changed due to the changes in transapical or pervalver axis length rather than apical length, i.e., the VA_{ratio} was affected by Fe′ and pCO_2 variation. These findings are in accordance with the previous study of six *Pseudo-nitzschia* strains that indicated that VA_{ratio} increased with decreasing iron availability (Marchetti and Harrison, 2007). However, the larger CV observed under low pCO_2 conditions is apparently a competitive disadvantage in CO_2-stressed environments. In the present study, the ρE_{SA} and its affinities were highest under low pCO_2 conditions, which can offset the growth disadvantage of a large CV. Therefore, the growth rate of *P. pseudodelicatissima* may not be affected by pCO_2 variations. Tortell et al. (2008) reported that the relative abundance of *Pseudo-nitzschia subcurvata* to *Chaetoceros* spp. (subgenus *Hyalochaete*) increased with a decrease in CO_2 (100 ppm xCO_2 bubbled). That finding partly supports our observation that *Pseudo-nitzschia* species can maintain their growth rates under low pCO_2 conditions.

Elemental composition. We demonstrated that the cellular elemental composition varied significantly under different pCO_2 and Fe′ conditions. With a few exceptions,

such as *Heterosigma akashiwo* (Raphidophyceae, Fu et al. 2008), phytoplankton C:N ratios are generally not affected by pCO_2 variation (Burkhardt et al. 1999, Sun et al. 2011), as observed in the present study. The constant C:N ratio of diatoms grown under different pCO_2 conditions suggests that the coupling of C and N metabolism is not affected by pCO_2 variations. In contrast, we found that the C:N ratio decreased with increasing iron availability. Bucciarelli et al. (2010) reported that the C:N ratio of the diatom *Thalassiosira oceanica* decreased with increasing in iron-limitation, but they were unable to detect a decreasing trend when evaluating compiled published data for 14 diatom species. Factors that alter the C:N ratio are related to growth conditions (e.g., temperature and light conditions) and show interspecific differences (Price 2005, Bucciarelli et al. 2010). In phytoplankton, iron-limitation leads to nitrogen co-limitation (Milligan and Harrison 2000) because iron is a cofactor of nitrate and nitrite reductases (Raven et al. 1999). The ratio of the iron coefficient in the regression in ρC_{SA} to that in ρN_{SA} was ~3.4 (Table 2), which is lower than the corresponding C:N ratio, suggesting a rapid decrease in N uptake activity relative to C uptake activity in response to a decrease in iron availability. Therefore, we conclude that a decrease in iron availability causes an increase in the C:N ratio of *P. pseudodelicatissima*.

When the pCO_2 was increased from ~200 to ~750 µatm, the C:P ratio increased by approximately 40% because ρP_{SA} decreased faster as pCO_2 increased than did ρC_{SA} (Fig. 4, Table 3). The elevation of the C:P ratio in diatoms and other phytoplankton under high pCO_2 conditions has previously been observed only under iron-replete conditions (e.g., Fu et al. 2008: *Prorocentrum minimum*, and King et al. 2011: *Attheya* sp.). Note that the contribution of extracellularly adsorbed phosphate was not affected by pCO_2 variation as examined using unialgal culture of the diatom *Chaetoceros* subgenus *Hyalochaete* (Sugie unpublished data). Within the intracellular fraction, the P-rich macromolecules responsible for cellular elemental compositions are RNA, DNA, and phospholipids (Geider and La Roche 2002). Specifically, the cellular RNA content increases as the growth rate of the diatom increases (Elser et al. 2003, Leonardos and Geider 2004). Our results indicate that the apparent nutrient uptake rates and iron uptake affinity were high under low pCO_2 conditions, but that the specific growth rate was not

449 significantly affected. Shi et al. (2010) reported that cadmium carbonic anhydrase, which
450 is a key component of CCMs, was upregulated at 160 ppm xCO_2 relative to 275–950
451 ppm xCO_2. It can be assumed that *P. pseudodelicatissima* is able to increase its RNA
452 synthesis under low pCO_2 conditions to upregulate nutrient and Fe uptake transporter
453 proteins and CCMs, such as carbonic anhydrase, resulting in a relatively low C:P ratio.
454 In the present study, the C:P ratio was not affected by iron availability (Table 2). In
455 contrast, Price (2005) reported that the C:P ratio of the diatom *T. weissflogii* increased
456 with increasing iron concentration; however, this trend was unclear at 50–100% of
457 $\mu:\mu_{max}$. Young and Beardall (2005) reported that a decrease in iron availability increased
458 the activity of CCMs in *Dunaliella tertiolecta* (Chlorophyceae), suggesting that
459 iron-limitation increases the C:P ratio through an increase in RNA synthesis. However,
460 the upregulation of CCMs in response to iron-limitation appears to be small compared to
461 that in response to a decrease in pCO_2 (e.g. Burkhardt et al. 2001, Trimborn et al. 2009).
462 However, the very limited information from very different taxa makes it difficult to
463 determine the effect of iron availability on the C:P ratio. The upregulation of CCMs may
464 require ATP, for which the C:P ratio is 10:3; nevertheless, the contribution of cellular P
465 derived from ATP appears to be much lower than that of other P-rich cellular constituents
466 (Geider and La Roche 2002). The C:P ratio of phytoplankton was previously reported to
467 be affected by phosphate and light availability (e.g. Diehl et al. 2005). However, we
468 believe that carbonate chemistry also contributes substantially to variation in the
469 canonical C:P value of 106 (Redfield et al. 1963). Furthermore, the atmospheric CO_2
470 concentration has changed dramatically over the geological time scale (Pearson and
471 Palmer 2000; Doney et al. 2009). Thus, we hypothesize that the observed change in C:P
472 value in response to pCO_2 variation of seawater plays a key role in the biogeochemical
473 cycling of oceanic P.
474 We found an increasing trend in the N:P ratio with increasing pCO_2. We predict
475 that the N:P ratio of phytoplankton will increase in the future with increasing pCO_2 in
476 oceans with high-CO_2. This, in turn, will lead to an increase in P availability in
477 P-limiting oligotrophic environments, that will result in an increase of N_2 fixation (c.f.
478 Moutin et al. 2008), the rate of which is significantly enhanced by an increase in pCO_2

(Hutchins et al. 2007, Levitan et al. 2007). However, the new production will decrease in N-limiting environments, where the iron concentration is sufficiently high to allow exhaustion of nutrients (e.g. Sugie et al. 2010a). These N-limiting environments are high productivity regions, including the majority of the coastal regions (Tyrrell and Law 1997, Wong et al. 2002). Unlike the C:P ratio, the N:P ratio was significantly affected by iron availability. As discussed above, iron availability has a greater effect on N assimilation than on C assimilation. The elevation of the N:P ratio in response to an increase in iron availability has been measured in unialgal culture of Antarctic diatom species (Timmermans et al. 2004, Timmermans and van der Wagt 2010). Changes in iron availability due to pH variations (Millero et al. 2009; Shi et al. 2010), which are difficult to predict, may modulate the trend in the N:P ratio observed in the present study.

We found that the Si:C, Si:N, and Si:P ratios varied according to the variations in pCO_2 and iron availability (Fig. 5). This finding supports the suggestion by Claquin et al. (2002) that the Si and other nutrient assimilation processes are uncoupled. Iron availability was previously reported to affect cellular Si content or the ratio of Si to other nutrients (e.g. Bucciarelli et al. 2010, Sugie et al. 2010b and references therein). However, there is very little information available about the effect of pCO_2 on silicification of diatoms. Previous studies using natural plankton communities detected no significant effect of pCO_2 change on Si dynamics (Feng et al. 2009, 2010). Sun et al. (2011) reported that the Si:C ratio and the Si cell quota of the diatom *P. multiseries* decreased with an increase in pCO_2 from ~220 to ~730 µatm, but were not significantly different between ~400 and ~730 µatm pCO_2. Si:C and Si:N ratios tend to decrease with increasing pCO_2, as observed in the present study; however, the possible mechanisms underlying the decrease in diatom Si content are largely uncertain. Milligan et al. (2004) reported that the intracellular Si efflux and frustule dissolution rates of the diatom *T. weissflogii* were higher under high pCO_2 conditions (~750 µatm) than under low pCO_2 condition (~100 µatm). Accordingly, further studies to determine the effects of carbonate chemistry on silicon dynamics are required. Moreover, under natural conditions, iron bioavailability and speciation will change with pH (Millero et al. 2009, Shi et al. 2010), and the iron concentration oscillates seasonally due to physical and biological dynamics

509 (e.g. Nishioka et al. 2007, 2011). These factors are critical for controlling the dynamics
510 of diatomaceous Si (Takeda 1998, Sugie et al. 2010b); however, it is difficult to predict
511 the direction of future changes in iron availability. To enable predictions of the future
512 environment, sufficient data regarding variations in pCO_2 and iron availability in the past
513 and present must be obtained.
514 *Oceanographic relevance*. The cellular elemental composition is primarily
515 changed through substrate limitation or depletion (Diehl et al. 2005, Marchetti and
516 Harrison 2007, Sugie et al. 2010b). In the present study, the cellular elemental
517 composition varied with changes in carbonate chemistry, and DIC is apparently a
518 non-limiting substrate for growth. Our results indicate that pCO_2 and iron availability
519 could influence the biogeochemical cycling of nutrients in future high-CO_2 oceans in a
520 manner similar to that observed for phytoplankton blooms and in the geologic past (e.g.
521 Pearson and Palmer 2000, Morel 2008). However, future iron bioavailability is difficult
522 to predict because of the uncertainty regarding the precise chemical properties of
523 iron-binding ligands. Understanding the changes in the binding affinity of iron ligands
524 and photoreactivity of iron-ligand complexes in response to declining pH are important
525 issues to predict the bioavailability of iron in future high-CO_2 oceans. The present study
526 provides a new method for evaluating the individual effects of pCO_2 and iron availability
527 on phytoplankton ecophysiology. This method, in combination with natural plankton
528 incubations, should provide a useful means for assessing the interactive effects of pCO_2
529 and iron.
530 Even though *Pseudo-nitzschia* is a cosmopolitan genus (Hasle 2002), *P.*
531 *pseudodelicatissima* strain used in the present study was isolated from a coastal region.
532 Marchetti and Harrison (2007) reported that iron-limitation induced trends in the
533 elemental composition of several *Pseudo-nitzschia* species were consistent between
534 coastal and oceanic isolates. However, Berge et al. (2010) suggested that oceanic species
535 might be more sensitive to variations in pCO_2 and pH. To evaluate future nutrient
536 biogeochemistry in oceans with high CO_2, studies of the interactive effects of ocean
537 acidification and iron availability using other phytoplankton species and natural plankton
538 communities are required. In particular, the elemental compositions and nutrient

539 drawdown ratios of natural plankton communities have rarely been shown to be affected
540 by pCO_2 variations (e.g. Feng et al. 2009, 2010), except for dissolved organic carbon
541 (DOC) production under nutrient-depleted conditions (Yoshimura et al. 2010) and
542 transparent exopolymer particle and DOC production in a mesocosm enclosure in
543 southern Norway (Riebesell et al. 2007). In order to clarify the overall trends in changes
544 in C and other nutrients biogeochemistry in the oceans in response to changes in
545 carbonate chemistry, we need to resolve the discrepancies between the data for natural
546 phytoplankton communities and those for unialgal cultures.
547
548 Acknowledgement
549 Two anonymous reviewers provided invaluable comments which significantly improved
550 this manuscript. The iron data in the medium was kindly provided by Dr. J. Nishioka of
551 Hokkaido Univ. We wish to thank Dr. H. Hattori of Tokai Univ. for taking SEM image of
552 the *Pseudo-nitzschia pseudodelicatissima*. We also thank A. Matsuoka of CERES Inc. for
553 analyzing POC and PN, and K. Sugita, A. Tsuzuku and N. Kageyama for their help on
554 maintaining our culture collection of marine phytoplankton. This work was conducted in
555 the framework of the Plankton Ecosystem Response to CO_2 Manipulation Study
556 (PERCOM) project and supported by the grants from CRIEPI (#060215) and
557 Grants-in-Aid for Scientific Research (#22681004).
558
559 References
560 Allen, J. F. 2003. Cyclic, pseudocyclic and noncyclic photophosphorylation: new links in
561 the chain. *Trends Plant Sci*. 8:15-9.
562 Beardall, J., Roberts, S., & Raven, J. A. 2005. Regulation of inorganic carbon acquisition
563 by phosphorus limitation in the green alga *Chlorella emersonii*. *Can. J. Bot.*
564 83:859–64.
565 Berge, T., Daugbjerg, N., Andersen, B. B., & Hansen, P. J. 2010. Effect of lowered pH on
566 marine phytoplankton growth rates. *Mar. Ecol. Prog. Ser.* 416:79–91.

Bucciarelli, E., Pondaven, P., & Sarthou, G. 2010. Effects of an iron-light co-limitation on the elemental composition (Si, C, N) of the marine diatoms *Thalassiosira oceanica* and *Ditylum brightwellii*. *Biogeosciences* 7:657–69.

Burkhardt, S., Zondervan, I., & Riebesell, U. 1999. Effect of CO_2 concentration on C:N:P ratio in marine phytoplankton: A species comparison. *Limnol. Oceanogr*. 44:683–90.

Burkhardt, S., Amoroso, G., Riebesell, U., & Sültemeyer, D. 2001. CO_2 and HCO_3^- uptake in marine diatom acclimated to different CO_2 concentrations. *Limnol. Oceanogr*. 46:1378–1391.

Claquin, P., Martin-Jézéquel, V., Kromkamp, J. C., Veldhuis, M. J. W., & Kraay, G. W. 2002. Uncoupling of silicon compared with carbon and nitrogen metabolisms and the role of the cell cycle in continuous culture of *Thalassiosira pseudonana* (Bacillariophyceae) under light, nitrogen, and phosphorus control. *J. Phycol.* 38:922–30.

Crutzen, P. J. 2002. Geology of mankind. *Nature* 415: 23.

de Baar, H. J. W. 1994. von Liebig's law of the minimum and plankton ecology. *Prog. Oceanogr*. 33:347–86.

de Baar, H. J. W., Boyd, P. W., Coale, K. H., Landry, M. R., Tsuda, A., Assmy, P., Bakker, D. C. E., Bozec, Y., Barber, R. T., Brzezinski, M. A., Buesseler, K. O., Boyé, M., Croot, P. L., Gervais, F., Gorbunov, Y., Harrison, P. J., Hiscock, W. T., Laan, P., Lancelot, C., Law, C. S., Levasseur, M., Marchetti, A., Millero, F. J., Nishioka, J., Nojiri, Y., van Oijen, T., Riebesell, U., Rijkenberg, M. J. A., Saito, H., Takeda, S., Timmermans, K. R., Veldhuis, M. J. W., Waite A. M., & Wong, C. S. 2005. Synthesis of iron fertilization experiments: From the Iron Age in the Age of Enlightenment. *J. Geophys. Res.* 110:C09S16, doi:10.1029/2004JC002601.

Doney, S. C., Fabry, V. J., Feely, R. A., & Kleypas, J. A. 2009. Ocean acidification: The other CO_2 problem. *Ann. Rev. Mar. Sci.* 1:169–92.

Diehl, S., Berger, S., & Wöhrl, R. 2005. Flexible nutrient stoichiometry mediates environmental influences on phytoplankton and its resources. *Ecology* 86:2931–45.

596 Edmond, J. W. 1970. High precision determination of titration alkalinity and total carbon
597 dioxide content of seawater by potentiometric titration. *Deep-Sea Res.* 17:737–50.
598 Elser, J. J., Acharya, K., Kyle, M., Cotner, J., Makino, W., Markow, T., Watts, T., Hobbie,
599 S., Fagan, W., Schade, J., Hood, J., & Sterner, R. W. 2003. Growth rate-stoichiometry
600 couplings in diverse biota. *Ecol. Lett.* 6:936–43.
601 Falkowski, P. G., Katz, M. E., Knoll, A. H., Quigg, A., Raven, J. A., Schofield, O., &
602 Taylor, F. J. R. 2004. The evolution of modern eukaryotic phytoplankton. *Science*
603 305:354–60.
604 Feng, Y., Hare, C. E., Leblanc, K., Rose, J. M., Zhang, Y., DiTullio, G. R., Lee, P. A.,
605 Wilhelm, S. W., Rowe, J. M., Sun, J., Nemcek, N., Gueguen, C., Passow, U., Benner,
606 I., Brown, C., & Hutchins, D. A. 2009. Effects of increased pCO_2 and temperature on
607 the North Atlantic spring bloom. I. The phytoplankton community and biogeochemical
608 response. *Mar. Ecol. Prog. Ser.* 388:13–25.
609 Feng, Y., Hare, C. E., Rose, J. M., Handy, S. M., DiTullio, G. R., Lee, P. A., Smith Jr., W.
610 O., Peloquin, J., Tozzi, S., Sun, J., Zhang, Y., Dunbar, R. B., Long, M. C., Sohst, B.,
611 Lohan, M., & Hutchins, D. A. 2010. Interactive effects of iron, irradiance and CO_2 on
612 Ross Sea phytoplankton. *Deep-Sea Res. I* 57:368–83.
613 Finkel, Z. V., Matheson, K. A., Regan, K. S., & Irwin, A. J. 2010a. Genotypic and
614 phenotypic variation in diatom silicification under paleo-oceanographic conditions.
615 *Geobiology* 8:433–45.
616 Finkel, Z. V., Beardall, J., Flynn, K. J., Quigg, A., Rees, T. A. V., & Raven, J. A. 2010b.
617 Phytoplankton in a changing world: cell size and elemental stoichiometry. *J. Plankton*
618 *Res.* 32:119–37.
619 Fu, F. X., Warner, M. E., Zhang, Y., Feng, Y., & Hutchins, D. A. 2007. Effects of
620 increased temperature and CO_2 on photosynthesis, growth, and elemental ratios in
621 marine *Synechococcus* and *Prochlorococcus* (Cyanobacteria). *J. Phycol.* 43:485–96.
622 Fu, F. X., Zhang, Y., Warner, M. E., Feng, Y., Sun, J., & Hutchins, D. A. 2008. A
623 comparison of future increased CO_2 and temperature effects on sympatric
624 *Heterosigma akashiwo* and *Prorocentrum minimum*. *Harmful Algae* 7:76–90.

625 Geider, R. J., & La Roche, J. 2002. Redfield revisited: variability of C:N:P in marine
626 microalgae and its biochemical basis. *Eur. J. Phycol*. 37:1–17.
627 Gerringa, L. J. A., de Baar, H. J. W., & Timmermans, K. R. 2000. A comparison of iron
628 limitation of phytoplankton in natural oceanic waters and laboratory media
629 conditioned with EDTA. *Mar. Chem*. 68:335–46.
630 Gradstein, F. M., Ogg, J. G., Smith, A. G., Bleeker, W., & Lourens, L. J. 2004. A new
631 Geologic Time Scale, with special reference to Precambrian and Neogene. *Episodes*
632 27:83–100.
633 Hasle, G. R. 2002. Are most of the domoic acid-producing species of the diatom genus
634 *Pseudo-nitzschia* cosmopolites? *Harmful Algae* 1:137–46.
635 Hasle, G. R., & Syvertsen, E. E. 1997. Marine diatoms. *In* Tomas C. R. [Ed.] *Identifying*
636 *Marine Phytoplankton*. Academic Press, London, pp. 5–385.
637 Healey, F. P. 1980. Slope of the Monod equation as an indicator of advantage in nutrient
638 competition. *Microb. Ecol.* 5:281–6.
639 Hopkinson, B. M., Xu, Y., Shi, D., McGinn, P. J., & Morel, F. M. M. 2010. The effect of
640 CO_2 on the photosynthetic physiology of phytoplankton in the Gulf of Alaska. *Limnol.*
641 *Oceanogr.* 55:2011–24.
642 Hopkinson, B. M., Dupont, C. L., Allen, A. E., & Morel, F. M. M. 2011. Efficiency of
643 the CO_2-concentrating mechanism of diatoms. *Proc. Natl. Acad. Sci. USA* 108:3830–7.
644 Hutchins, D. A., Fu, F. X., Zhang, Y., Warner, M. E., Feng, Y., Portune, K., Bernhardt, P.
645 W., & Mulholland, M. R. 2007. CO_2 control of *Trichodesmium* N_2 fixation,
646 photosynthesis, growth rates, and elemental ratios: Implications for past, present, and
647 future ocean biogeochemistry. *Limnol. Oceanogr.* 52:1293–304.
648 Hutchins, D. A., Mulholland, M. R., & Fu, F. X. 2009. Nutrient cycles and marine
649 microbes in a CO_2-enriched ocean. *Oceanography* 22:128–45.
650 King, A. L., Sañudo-Wilhelmy, S. A., Leblanc, K., Hutchins, D. A., & Fu, F. 2011. CO_2
651 and vitamin B_{12} interactions determine bioactive trace metal requirements of a
652 subarctic Pacific diatom. *ISME J.* 5:1388–96.
653 Kudo, I. 2003. Change in the uptake and cellular Si:N ratio in diatoms responding to the
654 ambient Si:N ratio and growth phase. *Mar. Biol.* 143:39–46.

655 Kuma, K., Nishioka, J., & Matsunaga, K. 1996. Controls on iron(III) hydroxide
656 solubility in seawater: The influence of pH and natural organic chelators. *Limnol.*
657 *Oceanogr.* 41:396–407.
658 Leonardos, N., & Geider, R. J. 2004. Responses of elemental and biochemical
659 composition of *Chaetoceros muelleri* to growth under varying light and
660 nitrate:phosphate supply ratios and their influence on critical N:P. *Limnol. Oceanogr.*
661 49:2105–14.
662 Levitan, O., Rosenberg, G., Setlik, I., Setlikova, E., Grigel, J., Klepetar, J., Prasil, O., &
663 Berman-Frank, I. 2007. Elevated CO_2 enhances nitrogen fixation and growth in the
664 marine cyanobacteria *Trichodesmium*. *Glob. Change Biol.* 13:531–8.
665 Mahowald, N. M., Engelstaedter, S., Luo, C., Sealy, A., Artaxo, P., Benitez-Nelson, C.,
666 Bonnet, S., Chen, Y., Chuang, P. Y., Cohen, D. D., Dulac, F., Herut, B., Johansen, A.
667 M., Kubilay, N., Losno, R., Maenhaut, W., Paytan, A., Prospero, J. M., Shank, L. M.,
668 & Siefert, R. L. 2009. Atmospheric iron deposition: global distribution, variability,
669 and human perturbations. *Annu. Rev. Mar. Sci*. 1:245–78.
670 Marchetti, A., & Harrison, P. J. 2007. Coupling changes in the cell morphology and the
671 elemental (C, N, and Si) composition of the pennate diatom *Pseudo-nitzschia* due to
672 iron deficiency. *Limnol. Oceanogr.* 52:2270–84.
673 Millero, F. J., Woosley, R., DiTrolio, B., & Waters, J. 2009. Effect of ocean acidification
674 on the speciation of metals in seawater. *Oceanography* 22:72–85.
675 Milligan, A. J., & Harrison, P. J. 2000. Effect of non-steady-state iron limitation on
676 nitrogen assimilatory enzymes in the marine diatom *Thalassiosira weissflogii*
677 (Bacillariophyceae). *J. Phycol.* 36:78–86.
678 Milligan, A. J., Varela, D. E., Brzezinski, M. A., & Morel, F. M. M. 2004. Dynamics of
679 silicon metabolism and silicon isotopic discrimination in a marine diatom as a
680 function of pCO_2. *Limnol. Oceanogr.* 49:322–9.
681 Morel, F. M. M. 2008. The co-evolution of phytoplankton and trace element cycles in the
682 oceans. *Geobiology* 6:318–24.

683 Moutin, T., Karl, D. M., Duhamel, S., Rimmelin, P., Van Mooy, B. A. S., & Claustre, H.
684 2008. Phosphate availability and the ultimate control of new nitrogen input by
685 nitrogen fixation in the tropical Pacific Ocean. *Biogeosciences*, 5:95–109.
686 Nagumo, T. 1995. Simple and safe cleaning methods for diatom samples. *Diatom* 10:88.
687 (in Japanese)
688 Nishioka, J., Ono, T., Saito, H., Nakatsuka, T., Takeda, S., Yoshimura, T., Suzuki, K.,
689 Kuma, K., Nakabayashi, S., Tsumune, D., Mitsudera, H., Johnson, W. K., & Tsuda, A.
690 2007. Iron supply to the western subarctic Pacific: Importance of iron export from the
691 Sea of Okhotsk. *J. Geophys. Res.* 112:C10012, doi:10.1029/2006JC004055.
692 Nishioka, J., Ono, T., Saito, H., Sakaoka, K., & Yoshimura, T. 2011. Oceanic iron supply
693 mechanisms which support the spring diatom bloom in the Oyashio region, western
694 subarctic Pacific. *J. Geophys. Res.* 116:C02021, doi:10.1029/2010JC006321.
695 Obata, H., Karatani, H., & Nakayama, E. 1993. Automated determination of iron in
696 seawater by chelating resin concentration and chemiluminescence detection. *Anal.*
697 *Chem.* 65:1524–8.
698 Paasche, E. 1980. Silicon content of five marine plankton diatom species measured with
699 a rapid filter method. *Limnol. Oceanogr.* 25:474–80.
700 Pearson, P. N., & Palmer, M. R. 2000. Atmospheric carbon dioxide concentrations over
701 the past 60 million years. *Nature* 406:695–9.
702 Price, N. M., Harrison, G. I., Hering, J. G., Hudson, R. J. M., Nirel, P. M. V., Palenik, B.
703 P., & Morel, F. M. M. 1988/89. Preparation and chemistry of the artificial algal culture
704 medium Aquil. *Biol. Oceanogr.* 6:443–61.
705 Price, N. M. 2005. The elemental stoichiometry and composition of an iron-limited
706 diatom. *Limnol. Oceanogr.* 50:1159–71.
707 Raven, J. A., Evans, M. C. W., & Korb, R. E. 1999. The role of trace metals in
708 photosynthetic electron transport in O_2-evolving organisms. *Photosynth. Res.*
709 60:111–49.
710 Redfield, A. C., Ketchum, B. H., & Richards, F. A. 1963. The influence of organisms on
711 the composition of seawater. *In* Hill, M.N. [Ed.] *The Sea. Vol. 2.* Wiley, New York, pp.
712 26–77.

713 Reinfelder, J. R. 2011. Carbon concentrating mechanisms in eukaryotic marine
714 phytoplankton. *Ann. Rev. Mar. Sci.* 3:291−315.
715 Riebesell, U., Schulz, K. G., Bellerby, R. G. J., Botros, M., Fritsche, P., Meyerhöfer, M.,
716 Neill, C., Nondal, G., Oschiles, A, Wohlers, J., & Zöllner, E. 2007. Enhanced
717 biological carbon consumption in a high CO_2 ocean. *Nature* 450:545−8.
718 Rost, B., Riebesell, U., Burkhardt, S., & Sültemeyer, D. 2003. Carbon acquisition of
719 bloom-forming marine phytoplankton. *Limnol. Oceanogr.* 48:55–67.
720 Saito, M. A., Goepfert, T. J., & Ritt, J. T. 2008. Some thoughts on the concept of
721 colimitation: Three definitions and the importance of bioavailability. *Limnol.*
722 *Oceanogr.* 53:276–90.
723 Sarthou, G., Timmermans, K. R., Blain, S., & Tréguer, P. 2005. Growth physiology and
724 fate of diatoms in the ocean: a review. *J. Sea Res.* 53:25–42.
725 Shi, D., Xu, Y., Hopkinson, B. M., & Morel, F. M. M. 2010. Effect of ocean acidification
726 on iron availability to marine phytoplankton. *Science* 327:676–9.
727 Solórzano, L., & Sharp, J. H. 1980. Determination of total dissolved phosphorus and
728 particulate phosphorus in natural waters. *Limnol. Oceanogr.* 25:754–8.
729 Sugie, K., & Kuma, K. 2008. Resting spore formation in the marine diatom
730 *Thalassiosira nordenskioeldii* under iron- and nitrogen-limited conditions. *J. Plankton*
731 *Res.* 30:1245–55.
732 Sugie, K., Kuma, K., Fujita, S., Nakayama, Y., & Ikeda, T. 2010a. Nutrient and diatom
733 dynamics during late winter and spring in the Oyashio region of the western subarctic
734 Pacific Ocean. *Deep-Sea Res. II* 57:1630–42.
735 Sugie, K., Kuma, K., Fujita, S., & Ikeda, T. 2010b. Increase in Si:N drawdown ratio due
736 to resting spore formation by spring bloom-forming diatoms under Fe- and N-limited
737 conditions in the Oyashio region. *J. Exp. Mar. Biol. Ecol.* 382:108–16.
738 Sugie, K., Kuma, K., Fujita, S., Ushizaka, S., Suzuki, K., & Ikeda, T. 2011. Importance
739 of intracellular Fe pools on growth of marine diatoms by using unialgal cultures and
740 the Oyashio region phytoplankton community during spring. *J. Oceanogr.* 67:183–96.
741 Sun, J., & Liu, D. 2003. Geometric models for calculating cell biovolume and surface
742 area for phytoplankton. *J. Plankton Res.* 25:1331–46.

743 Sun, J., Hutchins, D. A., Feng, Y., Seubert, E. L., Caron, D. A., & Fu, F. X. 2011. Effects
744 of changing pCO_2 and phosphate availability on domoic acid production and
745 physiology of the marine harmful bloom diatom *Pseudo-nitzschia multiseries*. *Limnol.*
746 *Oceanogr.* 56:829–40.
747 Sunda, W., & Huntsman, S. 2003. Effect of pH, light, and temperature on Fe-EDTA
748 chelation and Fe hydrolysis in seawater. *Mar. Chem*. 84:35–47.
749 Takeda, S. 1998. Influence of iron availability on nutrient consumption ratio of diatoms
750 in oceanic waters. *Nature* 393:774–7.
751 Thingstad, T. F., Øvreås, L., Egge, J. K., Løvdal, T., & Heldal, M. 2005. Use of
752 non-limiting substrates to increase size; a generic strategy to simultaneously optimize
753 uptake and minimize predation in pelagic osmotrophs? *Ecol. Lett.* 8:675–82.
754 Timmermans, K. R., van der Wagt, B., & de Baar, H. J. W. 2004. Growth rates,
755 half-saturation constants, and silicate, nitrate, and phosphate depletion in relation to
756 iron availability of four large, open-ocean diatoms from the Southern Ocean. *Limnol.*
757 *Oceanogr.* 49:2141–51.
758 Timmermans, K. R., & van der Wagt, B. 2010. Variability in cell size, nutrient depletion,
759 and growth rates of the Southern ocean diatom *Fragilariopsis kerguelensis*
760 (Bacillariophyceae) after prolonged iron limitation. *J. Phycol.* 46:497–506.
761 Tortell, P. D., Payne, C. D., Li, Y., Trimborn, S., Rost, B., Smith, W. O., Riesselman, C.,
762 Dunber, R. B., Sedwick, P., & DiTullio, G. R. 2008. CO_2 sensitivity of Southern Ocean
763 phytoplankton. *Geophys. Res. Lett.* 35:L04605, doi:10.1029/2007GL032583.
764 Trimborn, S., Lundholm, N., Thoms, S., Richter, K. U., Krock, B., Hansen, P. J., & Rost,
765 B. 2008. Inorganic carbon acquisition in potentially toxic and non-toxic diatoms: the
766 effect of pH-induced changes in seawater carbonate chemistry. *Physiol. Plantarum*
767 133:92–105.
768 Tyrrell, T., & Law, C. S. 1997. Low nitrate:phosphate ratios in the global ocean. *Nature*
769 387:793–6.
770 Wong, C. S., Waser, N. A. D., Nojiri, Y., Whitney, F. A., Page, J. S., & Zeng, J. 2002.
771 Seasonal cycles of nutrients and dissolved inorganic carbon at high and mid latitudes

772 in the North Pacific Ocean during the *Skaugran* cruises: determination of new
773 production and nutrient uptake ratios. *Deep-Sea Res*. 49:5317–38.
774 Yoshimura, T., Nishioka, J., Suzuki, K., Hattori, H., Kiyosawa, H., & Watanabe, Y. W.
775 2010. Impacts of elevated CO_2 on organic carbon dynamics in nutrient depleted
776 Okhotsk Sea surface waters. *J. Exp. Mar. Biol. Ecol.* 395:191–8.
777 Young, E. B., & Beardall, J. 2005. Modulation of photosynthesis and inorganic carbon
778 acquisition in a marine microalga by nitrogen, iron, and light availability. *Can. J. Bot*.
779 83:917–28.

778 Figure legends

779 Figure 1. Change in (A) specific growth rate (μ) and (B) cell volume (CV) against Fe′
780 concentration ($-\log_{10}$[Fe′] = pFe′) and pCO_2 and relationships between (C) μ
781 and CV, (D) CV and apical axis (A_{ax}), (E) CV and transapical or pervalver axis
782 (TP_{ax}), and (F) valve aspect ratio (VA_{ratio}: A_{ax} divided by TP_{ax}) and surface area
783 (SA) to CV ratio of *Pseudo-nitzschia pseudodelicatissima* grown under various
784 pCO_2 and iron conditions. Open circles in (A) and (B) represent scatter
785 diagram of mean of the beginning and end of pFe (x-axis) and pCO_2 (y-axis)
786 values. Data and error bars in (D) to (F) represent mean and ± 1SD (n = 20).
787 Solid and dotted lines in (C), (E) and (F) represent linear regression of the data
788 (mean value) and 95% CL of the regression, respectively. The regression
789 formulae are: (C) CV = 20.9 (± 5.0) × μ + 42.3 (± 8.0) ($F_{1,18}$ = 17.4, p = 0.001,
790 R^2 = 0.49), (E) TP_{ax} = 0.016 (± 0.000) × CV + 1.06 (± 0.04) ($F_{1,18}$ = 1008, p <
791 0.001, R^2 = 0.98), (F) SA/CV = 0.171 (± 0.007) × VA_{ratio} − 0.185 (± 0.070)
792 ($F_{1,18}$ = 513, p < 0.001, R^2 = 0.97).

793 Figure 2. The initial slope (α) of the regression of the specific growth rate against Fe′
794 concentration calculated by fitting the Monod model.

795 Figure 3. Change in intracellular concentrations of (A) C (mol L^{-1}), (B) N (mol L^{-1}) and
796 (C) P (mmol L^{-1}) and (D) Si content per surface area (mmol m^{-2}) of
797 *Pseudo-nitzschia pseudodelicatissima* against pCO_2 and $-\log_{10}$[Fe′] variations.
798 Open circles are the same representation as in Fig. 1A.

799 Figure 4. Change in net uptake rate (ρ) of the nutrients per unit surface area (SA). (A)
800 ρC_{SA} (mol m^{-2} d^{-1}), (B) ρN_{SA} (mol m^{-2} d^{-1}) and (C) ρP_{SA} (mmol m^{-2} d^{-1}) and
801 (D) ρSi_{SA} (mol m^{-2} d^{-1}) of *Pseudo-nitzschia pseudodelicatissima* against pCO_2
802 and $-\log_{10}$[Fe′] variations. Open circles are the same representation as in Fig.
803 1A.

804 Figure 5. Change in the cellular elemental composition of *Pseudo-nitzschia*
805 *pseudodelicatissima* against pCO_2 and $-\log_{10}$[Fe′] variations. (A) C:N, (B) C:P,
806 (C) N:P, (D) Si:N, (E) Si:C, and (F) Si:P ratio. Open circles are the same
807 representation as in Fig. 1A.

Table 1. Medium conditions at the start and end of the experiment. Treatment was represented as the CO_2 concentration of bubbled air (ppm) and Fe level from low (Fe1) to high (Fe5) condition. Data represent mean ± range of the duplicate bottles.

Treatment	Initial					End				
	Measured TA ($\mu mol\ kg^{-1}$)	Measured DIC ($\mu mol\ kg^{-1}$)	Calculated pCO_2 (μatm)	Calculated pH (total scale)	Calculated Fe' ($pmol\ L^{-1}$)	Measured TA ($\mu mol\ kg^{-1}$)	Measured DIC ($\mu mol\ kg^{-1}$)	Calculated pCO_2 (μatm)	Calculated pH (total scale)	Calculated Fe' ($pmol\ L^{-1}$)
171-Fe1	2335 ± 1.2	1959 ± 6.8	241.3 ± 8.1	8.24 ± 0.01	3.1 ± 0.2	2328 ± 0.1	1885 ± 3.3	179.5 ± 12	8.33 ± 0.00	5.0 ± 0.1
-Fe2	2338 ± 0.5	1963 ± 6.2	242.8 ± 6.1	8.23 ± 0.01	6.1 ± 0.3	2338 ± 13	1869 ± 2.6	163.2 ± 5.1	8.37 ± 0.01	12 ± 0.7
-Fe3	2337 ± 1.4	1973 ± 27	257.1 ± 32	8.22 ± 0.04	14 ± 3.0	2326 ± 3.5	1878 ± 3.0	175.8 ± 4.2	8.34 ± 0.01	26 ± 1.1
-Fe4	2337 ± 0.1	1965 ± 5.5	245.1 ± 5.9	8.23 ± 0.01	30 ± 1.2	2322 ± 1.8	1845 ± 21	155.4 ± 13	8.38 ± 0.03	64 ± 8.5
-Fe5	2336 ± 2.4	1975 ± 8.6	257.6 ± 7.9	8.21 ± 0.01	55 ± 2.7	2317 ± 2.3	1871 ± 11	175.6 ± 7.4	8.34 ± 0.01	103 ± 6.9
386-Fe1	2336 ± 2.2	2068 ± 3.9	397.9 ± 4.1	8.06 ± 0.00	3.6 ± 0.1	2326 ± 1.6	2042 ± 2.5	365.9 ± 2.0	8.09 ± 0.00	4.1 ± 0.0
-Fe2	2336 ± 0.8	2075 ± 0.3	414.1 ± 0.7	8.04 ± 0.00	6.8 ± 0.0	2328 ± 1.3	2034 ± 2.2	348.5 ± 1.9	8.11 ± 0.00	9.0 ± 0.1
-Fe3	2337 ± 0.0	2072 ± 1.8	404.6 ± 3.7	8.05 ± 0.00	18 ± 0.3	2320 ± 1.1	2005 ± 1.3	313.5 ± 3.2	8.14 ± 0.00	27 ± 0.5
-Fe4	2337 ± 1.2	2077 ± 3.2	413.8 ± 8.6	8.45 ± 0.01	34 ± 1.2	2345 ± 28	1971 ± 29	244.7 ± 7.3	8.23 ± 0.00	82 ± 2.3
-Fe5	2337 ± 0.2	2072 ± 0.8	402.9 ± 2.0	8.06 ± 0.00	71 ± 0.5	2315 ± 0.8	1946 ± 7.5	243.8 ± 7.5	8.23 ± 0.00	161 ± 8.0
614-Fe1	2339 ± 1.1	2148 ± 3.0	605.6 ± 14	7.90 ± 0.01	3.2 ± 0.1	2326 ± 2.8	2116 ± 0.7	536.0 ± 4.9	7.95 ± 0.00	3.9 ± 0.1
-Fe2	2338 ± 0.0	2147 ± 1.0	602.8 ± 3.5	7.91 ± 0.00	6.6 ± 0.1	2323 ± 2.2	2102 ± 7.7	506.2 ± 16	7.97 ± 0.01	8.5 ± 0.4
-Fe3	2337 ± 1.2	2144 ± 2.8	596.6 ± 13	7.91 ± 0.01	17 ± 0.6	2318 ± 2.8	2070 ± 0.7	435.4 ± 6.9	8.02 ± 0.01	27 ± 0.7
-Fe4	2341 ± 1.7	2148 ± 3.2	596.2 ± 5.6	7.91 ± 0.00	33 ± 0.4	2317 ± 1.2	2034 ± 6.7	363.5 ± 10	8.09 ± 0.01	71 ± 3.2
-Fe5	2340 ± 1.0	2148 ± 3.7	600.1 ± 9.6	7.91 ± 0.01	66 ± 1.6	2315 ± 0.9	2037 ± 13	372.0 ± 23	8.08 ± 0.02	138 ± 14
795-Fe1	2335 ± 2.1	2185 ± 3.0	770.1 ± 6.1	7.81 ± 0.00	3.1 ± 0.0	2330 ± 0.5	2164 ± 1.4	698.5 ± 4.5	7.85 ± 0.00	3.5 ± 0.0
-Fe2	2336 ± 1.2	2184 ± 1.3	761.6 ± 11	7.82 ± 0.01	6.3 ± 0.1	2333 ± 0.7	2161 ± 4.4	670.2 ± 15	7.86 ± 0.01	7.5 ± 0.2
-Fe3	2339 ± 0.5	2187 ± 0.6	762.2 ± 4.9	7.82 ± 0.00	16 ± 0.1	2332 ± 1.6	2138 ± 1.7	591.5 ± 1.0	7.91 ± 0.00	23 ± 0.0
-Fe4	2336 ± 2.4	2182 ± 1.6	748.6 ± 2.7	7.82 ± 1.00	32 ± 0.2	2326 ± 0.6	2091 ± 9.4	469.8 ± 25	8.00 ± 1.02	64 ± 5.4
-Fe5	2337 ± 1.9	2182 ± 0.9	744.5 ± 3.6	7.83 ± 0.00	65 ± 0.5	2324 ± 1.0	2113 ± 0.2	531.9 ± 2.9	7.95 ± 0.00	105 ± 1.0

Table 2. Change in specific growth rate, cell volume (CV), surface area (SA) to CV ratio, valve aspect ratio (VA_{ratio}; apical axis divided by transapical or pervalver axis length), net C, N, P and Si uptake rate (ρ) per SA, and elemental compositions against pCO_2 and pFe ($-\log_{10}$[Fe']) variations during the course of the experiment. Listed are the constant (a) and the coefficients (b and c) of regression equation of $y = a + b \times pCO_2 + c \times pFe'$. Asterisks represent the significance level of the constant and coefficients (*t*-test, df = 39 except for CV of df = 19); *: $p < 0.05$, **: $p < 0.01$. n.s.: not significant coefficient. The insignificant parameter (pCO_2 or pFe) was eliminated from the multi-regression analysis.

	a	b	c	Significance of the regression
Growth rate and cell size				
μ (d^{-1})	7.57^{**}	n.s.	-0.562^{**}	$F_{1,38} = 452$, $p < 0.001$, $R^2 = 0.82$
CV (μm^3)	197^{**}	$-1.90\times10^{-2*}$	-10.58^{**}	$F_{2,17} = 15.0$, $p < 0.001$, $R^2 = 0.60$
SA/CV (μm^{-1})	6.46×10^{-2}	$2.25\times10^{-4*}$	0.150^{**}	$F_{2,17} = 20.9$, $p < 0.001$, $R^2 = 0.68$
VA_{ratio}	−0.992	$1.11\times10^{-3*}$	0.909^{**}	$F_{2,17} = 22.3$, $p < 0.001$, $R^2 = 0.69$
Net elemental uptake rate per unit SA				
ρC_{SA} (mol m^{-2} d^{-1})	87.8^{**}	$-3.99\times10^{-3*}$	-6.76^{**}	$F_{2,37} = 89.0$, $p < 0.001$, $R^2 = 0.82$
ρN_{SA} (mol m^{-2} d^{-1})	25.1^{**}	n.s.	-1.99^{**}	$F_{1,38} = 133$, $p < 0.001$, $R^2 = 0.77$
ρP_{SA} (mmol m^{-2} d^{-1})	681^{**}	-0.129^{**}	-47.5^{**}	$F_{2,37} = 53.5$, $p < 0.001$, $R^2 = 0.73$
ρSi_{SA} (mol m^{-2} d^{-1})	12.8^{**}	$-1.77\times10^{-3**}$	-0.859^{**}	$F_{2,37} = 34.4$, $p < 0.001$, $R^2 = 0.63$
Elemental composition				
C:N	0.272	n.s.	0.554^{**}	$F_{1,38} = 143$, $p < 0.001$, $R^2 = 0.78$
C:P	86.1^{**}	$8.28\times10^{-2**}$	n.s.	$F_{1,38} = 20.0$, $p < 0.001$, $R^2 = 0.33$
N:P	49.8^{**}	$1.38\times10^{-2**}$	-3.37^{**}	$F_{2,37} = 14.5$, $p < 0.001$, $R^2 = 0.41$
Si:N	-2.77^{**}	$-3.47\times10^{-4**}$	0.398^{**}	$F_{2,37} = 139$, $p < 0.001$, $R^2 = 0.88$
Si:C	-3.97×10^{-2}	$-5.34\times10^{-5**}$	$1.75\times10^{-2**}$	$F_{2,37} = 61.0$, $p < 0.001$, $R^2 = 0.76$
Si:P	−19.7	$9.96\times10^{-3*}$	3.86^{*}	$F_{2,37} = 6.60$, $p = 0.004$, $R^2 = 0.22$

Table 3. Maximum rate ($E_{SA\text{-}max}$), half saturation constants for dissolved inorganic Fe (Fe'; k_ρ) and initial slope (α) of net C, N, P and Si uptake (ρ) per unit surface area (SA) which were calculated by fitting the data to Monod equation against Fe′ concentrations at each xCO$_2$ treatment. Data represent mean ± standard error (n = 10).

	Injected air xCO$_2$ (ppm)	$\rho E_{SA\text{-}max}$ (mol m^{-2} d^{-1})	k_ρ (pmol Fe' L^{-1})	α	Significance of Monod model
ρC_{SA}	171	19.5 ± 0.6	4.8 ± 0.7	4.10	$F_{1,8} = 1358$, $p < 0.001$, $R^2 = 0.93$
	386	19.1 ± 0.5	5.7 ± 0.7	3.33	$F_{1,8} = 1430$, $p < 0.001$, $R^2 = 0.96$
	614	17.3 ± 1.1	5.0 ± 1.4	3.45	$F_{1,8} = 263$, $p < 0.001$, $R^2 = 0.82$
	795	18.1 ± 0.8	5.6 ± 1.1	3.24	$F_{1,8} = 570$, $p < 0.001$, $R^2 = 0.92$
ρN_{SA}	171	5.3 ± 0.2	4.9 ± 0.8	1.07	$F_{1,8} = 1173$, $p < 0.001$, $R^2 = 0.92$
	386	5.6 ± 0.3	6.1 ± 1.2	0.92	$F_{1,8} = 494$, $p < 0.001$, $R^2 = 0.89$
	614	4.8 ± 0.3	5.0 ± 1.5	0.97	$F_{1,8} = 239$, $p < 0.001$, $R^2 = 0.80$
	795	5.1 ± 0.3	5.6 ± 1.2	0.92	$F_{1,8} = 433$, $p < 0.001$, $R^2 = 0.89$
ρP_{SA}	171	0.19 ± 0.01	3.6 ± 1.0	0.052	$F_{1,8} = 514$, $p < 0.001$, $R^2 = 0.77$
	386	0.19 ± 0.02	8.2 ± 2.8	0.023	$F_{1,8} = 156$, $p < 0.001$, $R^2 = 0.78$
	614	0.12 ± 0.01	3.6 ± 1.2	0.031	$F_{1,8} = 231$, $p < 0.001$, $R^2 = 0.70$
	795	0.12 ± 0.00	4.7 ± 0.6	0.026	$F_{1,8} = 1177$, $p < 0.001$, $R^2 = 0.95$
ρSi_{SA}	171	4.1 ± 0.1	3.3 ± 0.6	1.22	$F_{1.8} = 1244$, $p < 0.001$, $R^2 = 0.88$
	386	3.6 ± 0.2	2.6 ± 0.8	1.36	$F_{1,8} = 350$, $p < 0.001$, $R^2 = 0.67$
	614	3.3 ± 0.3	3.4 ± 1.5	0.97	$F_{1,8} = 151$, $p < 0.001$, $R^2 = 0.61$
	795	3.1 ± 0.2	3.2 ± 0.9	0.96	$F_{1,8} = 374$, $p < 0.001$, $R^2 = 0.80$

Figure 1

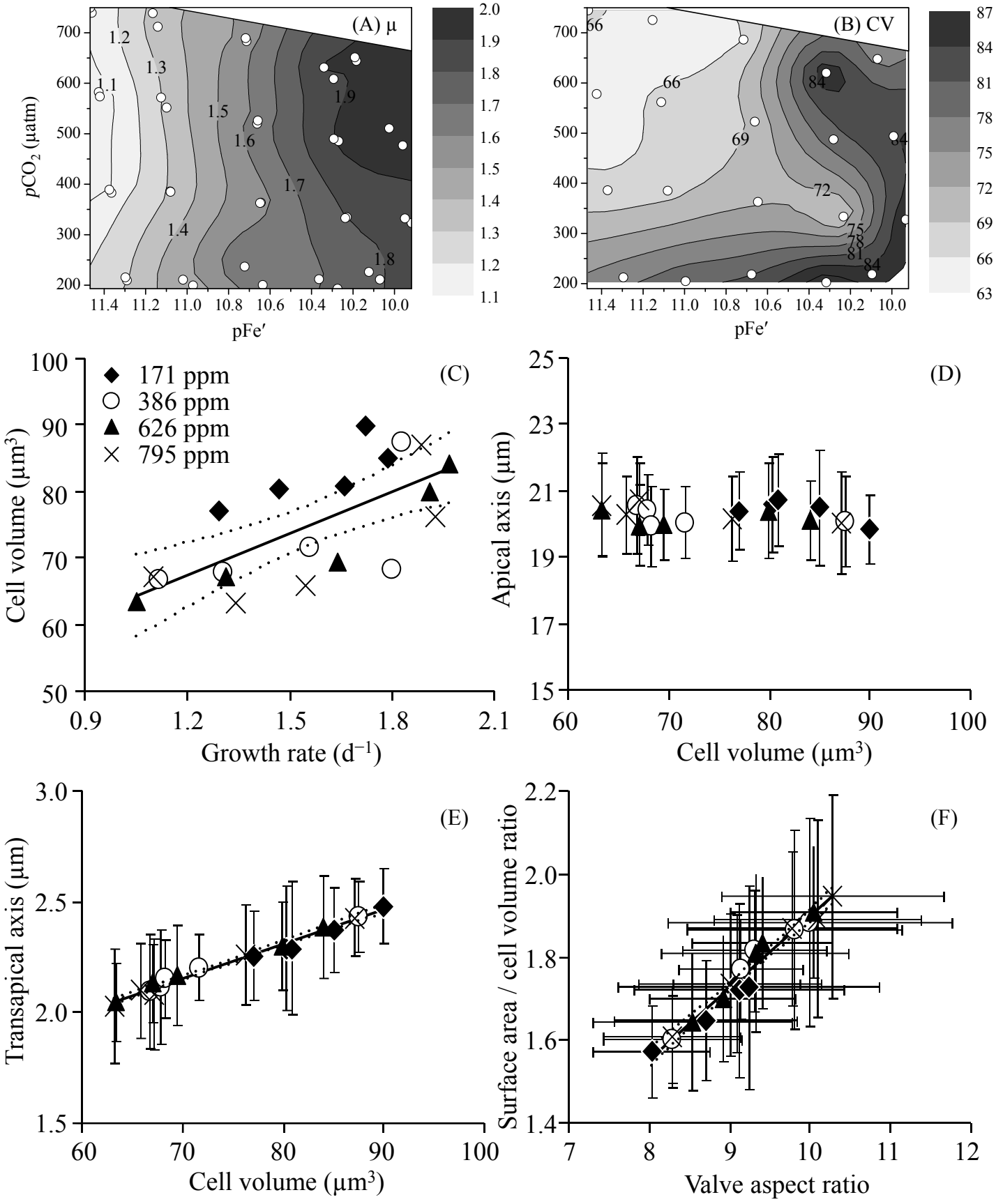
(A) μ
(B) CV
pCO2 (μatm)
pFe′
(C)
171 ppm
386 ppm
626 ppm
795 ppm
Cell volume (μm3)
Growth rate (d−1)
(D)
Apical axis (μm)
Cell volume (μm3)
(E)
Transapical axis (μm)
Cell volume (μm3)
(F)
Surface area / cell volume ratio
Valve aspect ratio

Figure 2

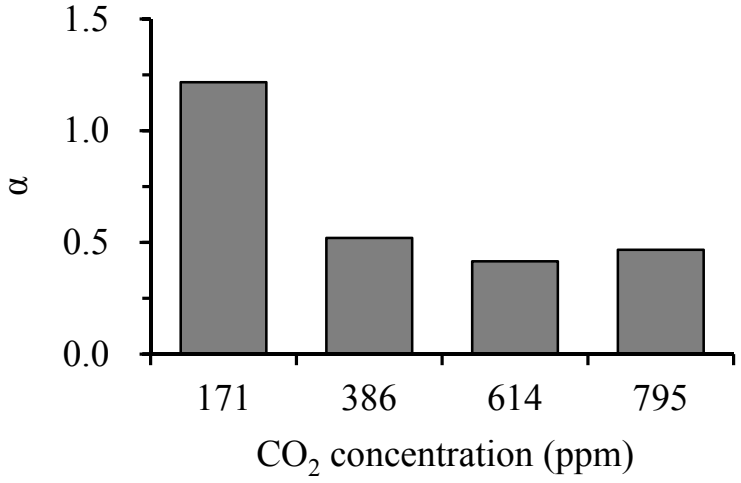

Figure 3

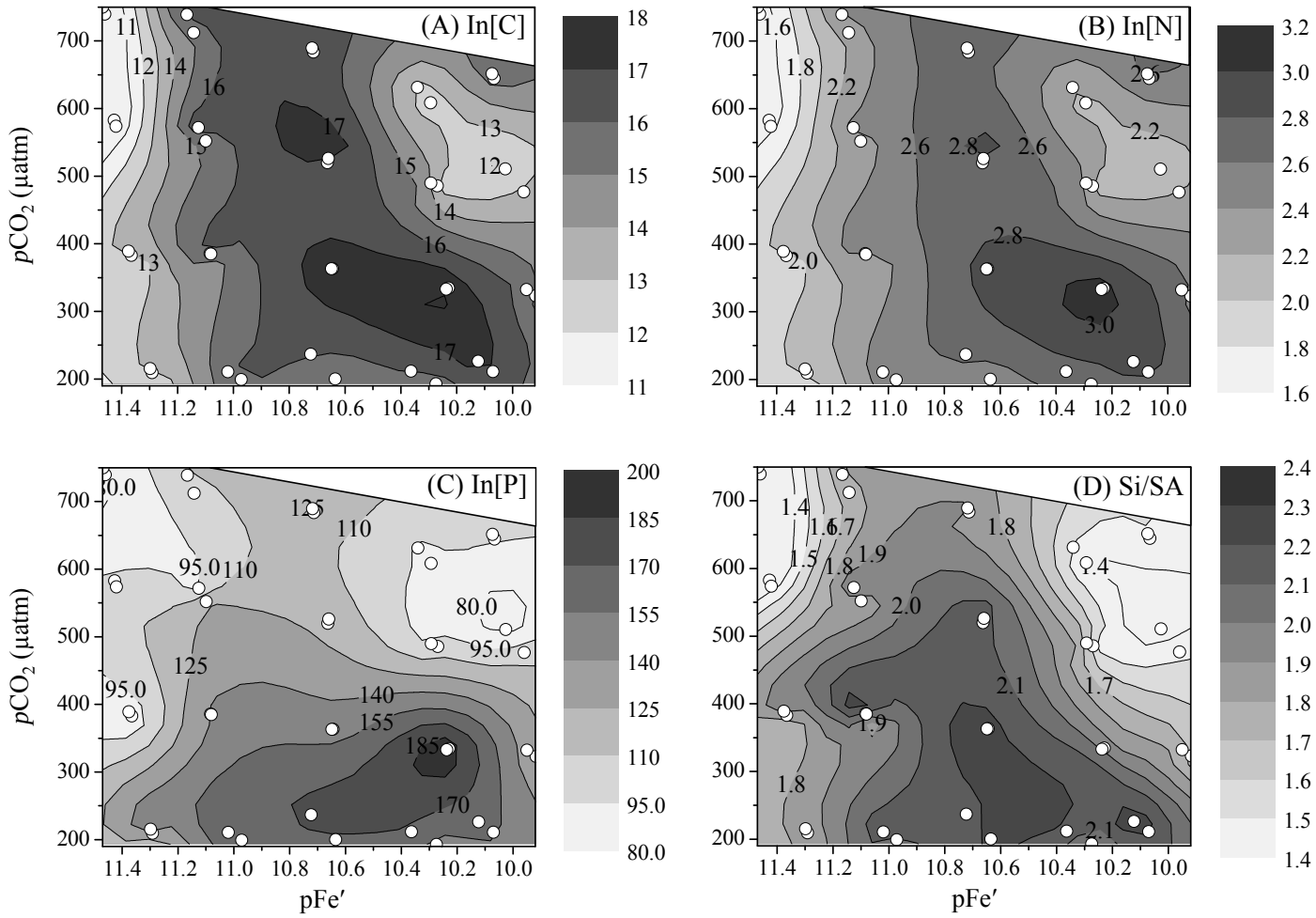
(A) In[C]
(B) In[N]
(C) In[P]
(D) Si/SA
pCO2 (µatm)
pFe′
700
600
500
400
300
200
11.4
11.2
11.0
10.8
10.6
10.4
10.2
10.0

Figure 4

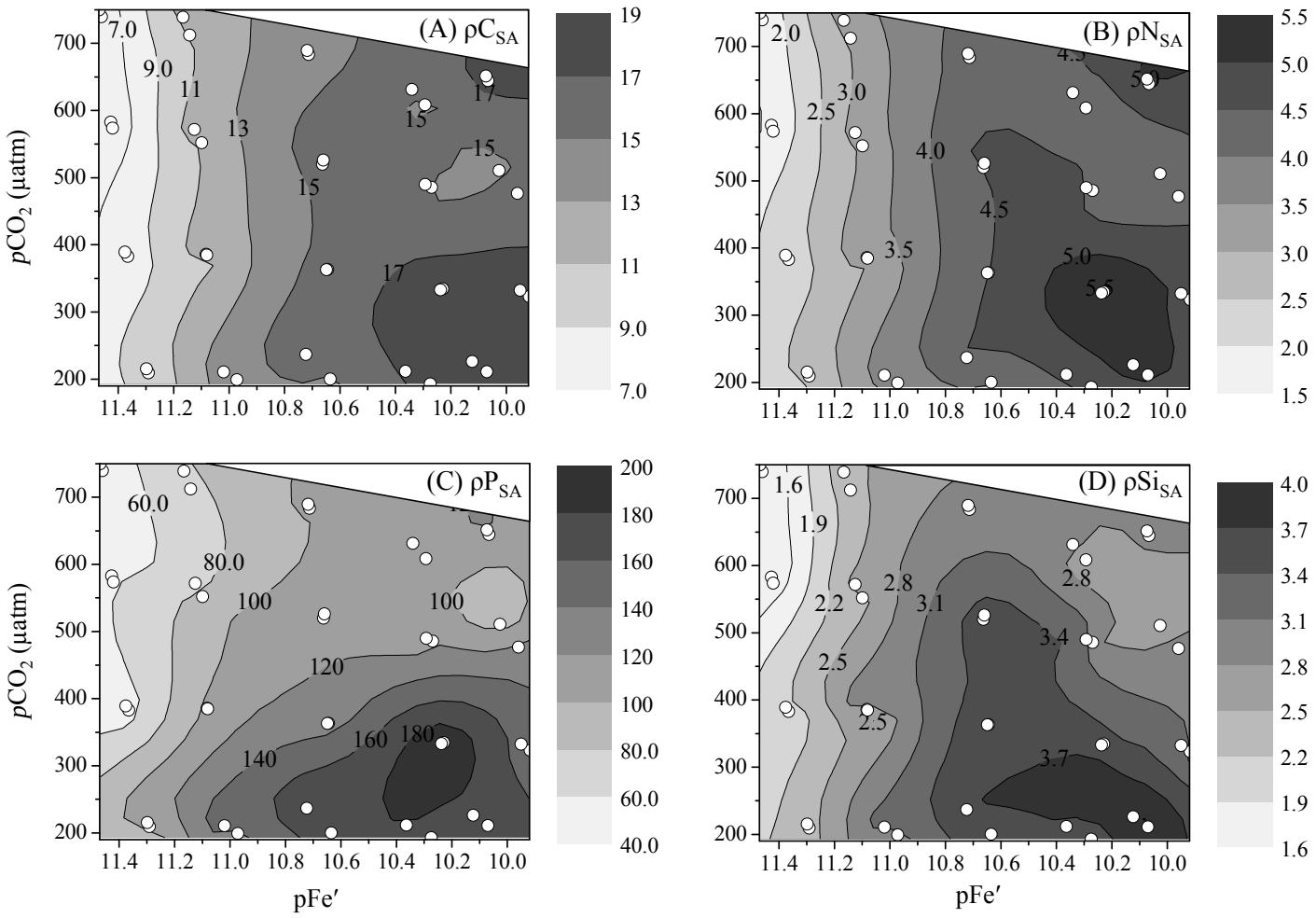
(A) ρC$_{SA}$
(B) ρN$_{SA}$
(C) ρP$_{SA}$
(D) ρSi$_{SA}$
pCO$_2$ (μatm)
pFe′
700
600
500
400
300
200
11.4
11.2
11.0
10.8
10.6
10.4
10.2
10.0
7.0
9.0
11
13
15
17
19
2.0
2.5
3.0
3.5
4.0
4.5
5.0
5.5
1.5
60.0
80.0
100
120
140
160
180
200
40.0
1.6
1.9
2.2
2.5
2.8
3.1
3.4
3.7
4.0

Figure 5